Geophysical Research Letters

RESEARCH LETTER
10.1029/2019GL082681

On How High-Latitude Chorus Waves Tip the Balance Between Acceleration and Loss of Relativistic Electrons

Dedong Wang[1] **and Yuri Y. Shprits**[1,2,3]

[1]Section 2.8 Magnetospheric Physics, GFZ German Research Centre for Geosciences, Potsdam, Germany, [2]Institute of Physics and Astronomy, University of Potsdam, Potsdam, Germany, [3]Department of Earth, Planetary, and Space Sciences, University of California, Los Angeles, CA, USA

Key Points:
- The high-latitude chorus waves can tip the balance between acceleration and loss of relativistic electrons at MeV energies
- Depending on their latitudinal distribution, chorus waves can produce net acceleration or net loss of MeV electrons
- Variations in high-latitude chorus may account for some of the variability of MeV electrons

Supporting Information:
- Supporting Information S1

Correspondence to:
D. Wang,
dedong@gfz-potsdam.de

Citation:
Wang, D., & Shprits, Y. Y. (2019). On how high-latitude chorus waves tip the balance between acceleration and loss of relativistic electrons. *Geophysical Research Letters*, *46*, 7945–7954. https://doi.org/10.1029/2019GL082681

Received 6 MAR 2019
Accepted 29 JUN 2019
Accepted article online 8 JUL 2019
Published online 30 JUL 2019

Abstract Modeling and observations have shown that energy diffusion by chorus waves is an important source of acceleration of electrons to relativistic energies. By performing long-term simulations using the three-dimensional Versatile Electron Radiation Belt code, in this study, we test how the latitudinal dependence of chorus waves can affect the dynamics of the radiation belt electrons. Results show that the variability of chorus waves at high latitudes is critical for modeling of megaelectron volt (MeV) electrons. We show that, depending on the latitudinal distribution of chorus waves under different geomagnetic conditions, they cannot only produce a net acceleration but also a net loss of MeV electrons. Decrease in high-latitude chorus waves can tip the balance between acceleration and loss toward acceleration, or alternatively, the increase in high-latitude waves can result in a net loss of MeV electrons. Variations in high-latitude chorus may account for some of the variability of MeV electrons.

1. Introduction

Whistler-mode chorus waves are suggested to play an important role in the dynamic evolution of radiation belt electrons (e.g., Horne & Thorne, 1998, 2003; Millan & Baker, 2012; Shprits et al., 2008; Summers et al., 1998; Thorne, 2010; Xiao et al., 2010, 2015). In recent years, the effect of chorus waves on net acceleration of electrons in radiation belts has been studied extensively (e.g., Horne & Thorne, 1998; Reeves et al., 2013; Thorne et al., 2013; Xiao et al., 2014). A number of studies concluded that the net effect of chorus waves on the radiation belt electrons at megaelectron volt (MeV) energies is acceleration (e.g., Horne et al., 2005; Li et al., 2007; Shprits et al., 2008; Su et al., 2014; Thorne, 2010; Tu et al., 2013; Turner et al., 2014; Xiao et al., 2009). However, depending on the latitudinal distribution of chorus waves, chorus waves can cause not only acceleration but also loss of relativistic electrons (e.g., Horne & Thorne, 2003). Shprits et al. (2006) and Thorne et al. (2005) suggested that chorus waves confined to low latitudes cannot produce significant loss of MeV electrons. However, when chorus waves with the same spectral properties extend to higher geomagnetic latitudes, for example, above 30°, they are capable of producing very fast loss of the relativistic electrons on the scale of 1 day. Thus, the latitudinal distribution of chorus waves plays an important role in the dynamic evolution of radiation belt electrons. To evaluate the net effect of chorus waves on MeV electrons, one needs to solve the full 3-D Fokker-Planck equation which requires computing bounce- and magnetic local time (MLT)-averaged diffusion coefficients due to chorus waves. Diffusion of particles depends on gradients in phase space and diffusion coefficients (e.g., Allison et al., 2019). Computation of diffusion coefficients needs chorus wave models depending on MLT, latitude, L, and geomagnetic conditions (Shprits et al., 2008). Early observations showed that chorus waves mainly occur in two magnetic latitude regions: one near the equator ($|\lambda| \leq 15°$) on the nightside and the other at higher latitudes ($|\lambda| > 15°$) on the dayside (e.g., Tsurutani & Smith, 1977). Recent observations show that chorus waves on the dayside can extend to latitudes up to 30° and possibly beyond (e.g., Agapitov et al., 2015, 2018; Bunch et al., 2013; Meredith et al., 2003, 2004; Santolík et al., 2014). A number of statistical models of chorus waves have been recently developed (e.g., Li et al., 2007; Horne et al., 2013; Meredith et al., 2012). Using more than 5 years of Van Allen Probe data, the functional dependences of chorus waves on L, MLT, magnetic latitude, and geomagnetic condition have been developed (Wang et al., 2019). However, the measurements from Van Allen Probes are limited to low geomagnetic latitudes ($< 20°$). Combining 10 years of Cluster (2001–2010) and Van Allen Probes data, Agapitov et al. (2018) developed a synthetic empirical chorus wave model. However,

the coverage of Cluster data in the inner magnetosphere is limited as satellites spend most of their time in the outer magnetosphere. The wave instruments on board the Van Allen Probes and Cluster have a different resolution, sensitivity, and frequency range, which result in more uncertainties for the modeling work.

In this study, to investigate the sensitivity of the distribution of high-latitude (20–45°) chorus waves on the dynamic evolution of the radiation belt electrons at MeV energies, we perform 3-D simulations, including pitch angle, energy, and mixed diffusion, for 1 year, from 1 October 2012 to 1 October 2013, which includes multiple storm time and non–storm time periods. Recent studies show that electromagnetic ion cyclotron (EMIC) waves play an important role in the dynamics of multi-MeV electrons (with energies higher than several MeV), while electrons with lower energy (below ~1 MeV) are unaffected by EMIC waves (e.g., Drozdov et al., 2015; Kersten et al., 2014; Shprits et al., 2013, 2016, 2017; Wang et al., 2014; Usanova et al., 2014). By taking the hot plasma effects into account, Cao et al. (2017) shows that the electron minimum resonant energy for cyclotron resonant interactions with EMIC waves is typically larger than 2 MeV. To avoid the potential contribution of the EMIC waves, in our study, we focus on the effect of chorus waves on the dynamic evolution of relativistic electrons at 0.9 MeV energy. In section 2, we describe the three-dimensional Versatile Electron Radiation Belt (VERB-3D) code and the parameters adopted for the numerical simulations. In section 3, we perform two test simulations and compare the results with satellite observations. One of the simulations adopts chorus waves at absolute geomagnetic latitude lower than 20°, and the other simulation uses chorus waves extending to 45°. We summarize and discuss our results and outline a road map for future studies in section 4.

2. Model Description

The dynamic evolution of electrons in the radiation belts can be described by the bounce- and MLT-averaged Fokker-Planck equation (e.g., Shprits et al., 2009; Schulz & Lanzerotti, 1974):

$$\frac{\partial f}{\partial t} = L^{*2}\frac{\partial}{\partial L^*}\bigg|_{\mu,J}\left(\frac{1}{L^{*2}}D_{L^*L^*}\frac{\partial f}{\partial L^*}\bigg|_{\mu,J}\right) + \frac{1}{p^2}\frac{\partial}{\partial p}\bigg|_{\alpha_0,L^*}p^2\left(D_{pp}\frac{\partial f}{\partial p}\bigg|_{\alpha_0,L^*} + D_{p\alpha_0}\frac{\partial f}{\partial \alpha_0}\bigg|_{p,L^*}\right) + \frac{1}{T(\alpha_0)\sin\quad(2\alpha_0)}\frac{\partial}{\partial \alpha_0}\bigg|_{p,L^*}T(\alpha_0)\sin(2\alpha_0)\left(D_{\alpha_0\alpha_0}\frac{\partial f}{\partial \alpha_0}\bigg|_{p,L^*} + D_{\alpha_0 p}\frac{\partial f}{\partial p}\bigg|_{\alpha_0,L^*}\right) - \frac{f}{\tau_{lc}}, \tag{1}$$

where f is the electron phase space density (PSD); μ and J are the first and second adiabatic invariants; p is the relativistic momentum; α_0 is the equatorial pitch angle of the particles, and $T(\alpha_0)$ is a function related to the bounce frequency, which can be approximated as (Lenchek & Singer, 1962)

$$T(\alpha_0) = 1.3802 - 0.3198(\sin\alpha_0 + \sin^{1/2}\alpha_0). \tag{2}$$

$D_{L^*L^*}$, D_{pp}, $D_{p\alpha_0}$, $D_{\alpha_0 p}$, and $D_{\alpha_0\alpha_0}$ in equation (1) are the bounce- and MLT-averaged scattering rates (or diffusion coefficients) due to resonant wave-particle interactions. In the following part of this section, we describe how the diffusion coefficients are calculated, the methodology we used in the simulations, and the method we adopted to validate our simulation results against the satellite observations.

2.1. Diffusion Coefficients

The radial diffusion coefficient due to the interaction with ultralow-frequency waves is adopted from Brautigam and Albert (2000):

$$D_{L^*L^*}(Kp, L^*) = 10^{(0.506Kp-9.325)}L^{*10}. \tag{3}$$

This parameterization is valid for $Kp \leq 6$. However, in this study, we extrapolate it and use it for all Kp values. Similar results are obtained using the radial diffusion coefficients from Ozeke et al. (2014; not shown in the manuscript). Bounce- and MLT-averaged diffusion coefficients D_{pp}, $D_{p\alpha_0}$, $D_{\alpha_0 p}$, and $D_{\alpha_0\alpha_0}$ are calculated using the Full Diffusion Code (FDC; Orlova & Shprits, 2011; Ni et al., 2008; Shprits & Ni, 2009). For the wave normal angle (θ) distribution of chorus waves, we use a frequently adopted model, that is, $\theta_{lc} = 0°, \theta_{uc} = 45°, \theta_m = 0°$, and $\theta_w = 30°$, where θ_m is the peak value of wave normal angle, θ_w is the width of the angle, and θ_{lc} and θ_{uc} are the lower and upper cutoff to the wave normal angle distribution, outside which the wave power is 0 (e.g., Kim et al., 2012; Thorne et al., 2013). Recent studies suggest that highly oblique chorus waves with wave normal angle near 70° may contribute to the dynamic evolution of

radiation belt electrons (e.g., Agapitov et al., 2018; Artemyev et al., 2016). However, Santolík et al. (2014) found that intense chorus waves are mostly field aligned. Investigating the effect of highly oblique chorus waves is beyond the scope of current study and will be a topic in the future work. For the amplitude and frequency distribution of chorus waves at low latitudes, we employ the newly developed model by Wang et al. (2019) based on more than 5 years of Van Allen Probe data. For high-latitude chorus waves, we extend chorus waves up to 45° latitude during geomagnetic quiet times, assuming that amplitudes of chorus waves at latitudes from 20° to 45° are the same as the amplitudes at 20° latitude, which is consistent with the observations from Cluster (Agapitov et al., 2018). The chorus wave model from Wang et al. (2019) depends on L, MLT, magnetic latitude, and geomagnetic conditions. On the nightside, chorus waves are confined to low latitudes, and the model provides amplitude of chorus waves at 20° latitude close to 0 pT (see their Figures 11 and 12). Thus, nightside chorus waves are confined to low latitudes in our simulations. On the dayside, amplitudes of lower-band chorus waves at low latitudes increase with latitude (see Figure 12i in Wang et al., 2019). Therefore, only chorus waves on the dayside are extended to high latitudes. For chorus waves at high latitudes, as shown in Figures 5–7 in Agapitov et al. (2018), the root-mean-square values of chorus wave amplitude remain relatively similar at high latitudes in the same MLT/L sector and geomagnetic conditions. Following their study, for high-latitude chorus waves, we also divide geomagnetic conditions to three levels: $Kp > 4$, $2 \leq Kp \leq 4$, and $Kp < 2$. During each geomagnetic level, it can be seen from their Figure 5 that amplitudes of chorus waves on the dayside are relatively similar. Thus, we calculate diffusion coefficients of chorus waves at high latitudes in each MLT and L when $Kp = 4$ and implement these diffusion coefficients for high-latitude chorus waves when $2 \leq Kp \leq 4$. MLT- and bounce-averaged diffusion coefficients due to low- and high-latitude chorus waves at $L = 6$, $Kp = 4$ are shown in supporting information Figure S1. When Kp is higher than 4, it is assumed that chorus waves are strongly damped at high latitudes during storms and are not present at latitudes above 20°. This assumption is based on the consideration that the damping of chorus waves at high latitudes could increase with geomagnetic disturbances (Chen et al., 2013). During quiet times when $Kp < 2$, we scale the calculated diffusion coefficients for high-latitude chorus waves with a factor of 0.8. This scaling factor is based on the consideration that amplitudes of high-latitude chorus waves only decrease slightly with decreasing Kp when Kp is lower than 4, as shown in Figures 5–7 of Agapitov et al. (2018). For the plasmaspheric hiss waves, we use a model based on Van Allen Probe observations (Orlova et al., 2016; Spasojevic et al., 2015). In this study, we assume local diffusion due to chorus waves outside the plasmasphere and due to hiss waves inside the plasmasphere. Effects of lightning whistlers are also included with the same parameterization as in Kim et al. (2012).

2.2. Simulation Methodology

Apart from diffusion coefficients, a number of critical boundaries are also dynamically changing in our simulations. First of all, the location of the plasmapause is calculated using the time series of the Kp index according to Carpenter and Anderson (1992) as follows:

$$L_{pp} = 5.6 - 0.46\mathrm{Kp}_{\max}, \tag{4}$$

where L_{pp} is the location of the plasmapause, and $Kp_{\max}$ is the maximum Kp value over the previous 24 hr. The last closed drift shell is calculated using the IRBEM library and (Boscher et al., 2010) the TS07D magnetic field model (Tsyganenko & Sitnov, 2007) and is used to model the effect of magnetopause shadowing. When L^* is higher than the last closed drift shell, we set the PSD to be 0. The flux variation at the outer boundary ($L^* = 6.6$) is taken from the measurements from the Geostationary Operational Environmental Satellite (GOES). First, we calculated the PSD of electrons from GOES particle data using TS07D magnetic field model. Then, we did daily average over the calculated PSD, and assume that the PSD at $L^* = 6.6$ is approximately the same as PSD at the daily averaged L^* of GOES, since at high L^* the radial diffusion is strong (Brautigam & Albert, 2000). The initial condition is set up using a steady-state solution of radial diffusion and prescribed loss. All of these settings, except for explicit handling of the magnetopause loss, are the same as in previous studies that should be referred to for more technical details of the VERB-3D code (e.g., Drozdov et al., 2017; Kim et al., 2012; Shprits et al., 2009; Subbotin et al., 2011).

2.3. Validation Methodology

In this study, we validate our simulation results against satellite observations using normalized difference (ND) between them, which is defined as

$$\mathrm{ND}(L^*, t) = 2 * \frac{J_S(L^*, t) - J_O(L^*, t)}{J_S(L^*, t) + J_O(L^*, t)}, \tag{5}$$

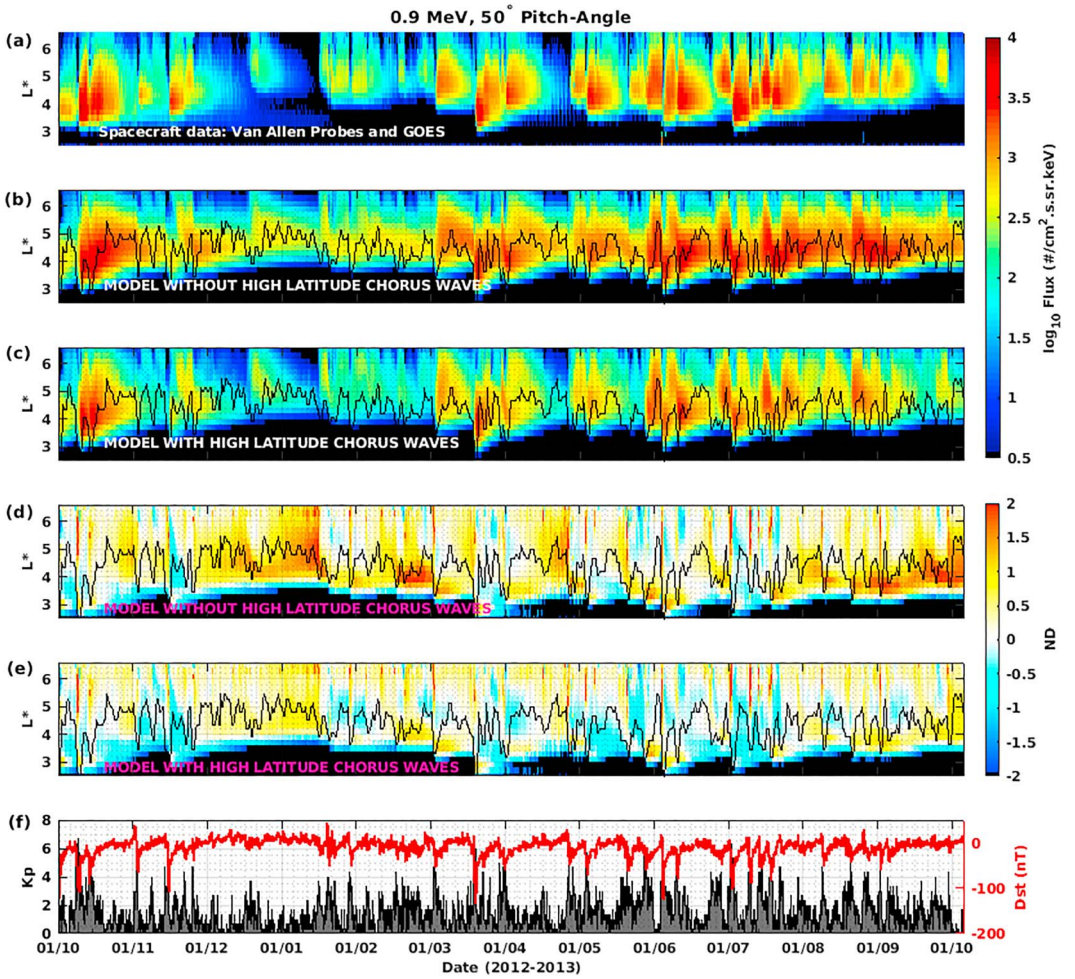

Figure 1. Particle observations and VERB-3D simulations from 1 October 2012 to 1 October 2013. (a) Particle flux electrons of 0.9 MeV with 50° pitch angle from observations of Van Allen Probes A and B and GOES 13 and 15. (b) VERB-3D Simulation 1 for this period. In this simulation, chorus waves are limited to low latitudes (20°). (c) VERB-3D Simulation 2 for the same period as in panel (b), but chorus waves extended to 45° using assumed activity dependence of chorus waves at high latitudes. (d) Normalized difference between the satellite data and Simulation 1. (e) Normalized difference between the satellite data and Simulation 2. (f) *Dst* and *Kp* index in this period. The overplotted black lines in panels (b)–(e) show the plasmapause location. VERB-3D = three-dimensional Versatile Electron Radiation Belt.

where J_S is the simulated flux and J_O is the observed flux. To show the major differences between observations and simulations or between different simulations, we also calculated the differences normalized by the average maximum flux for each given time ($\mathrm{ND}_{\max}(L^*, t)$), which is defined as

$$\mathrm{ND}_{\max}(L^*, t) = \frac{J_1(L^*, t) - J_2(L^*, t)}{\max|_{\text{over } L^* \text{ at constant } t} \frac{J_1(L^*, t) + J_2(L^*, t)}{2}}, \quad (6)$$

where J_1 and J_2 are the flux from observations and simulations or the flux from different simulations. In the supporting information, we also show the logarithmic difference quantifying the difference between observations and simulations.

3. Sensitivity Test for High-Latitude Chorus Waves

To explore the effect of high-latitude chorus waves, in this letter we first show two long-term simulations from 1 October 2012 to 1 October 2013, including several storm and nonstorm periods. Except for the distribution of high-latitude chorus waves, all the other setup parameters are the same for these simulations. For low-latitude chorus waves, both simulations use the chorus wave model derived from Van Allen Probe observations (Wang et al., 2019). In the first simulation, we limit the maximum latitude of chorus waves at

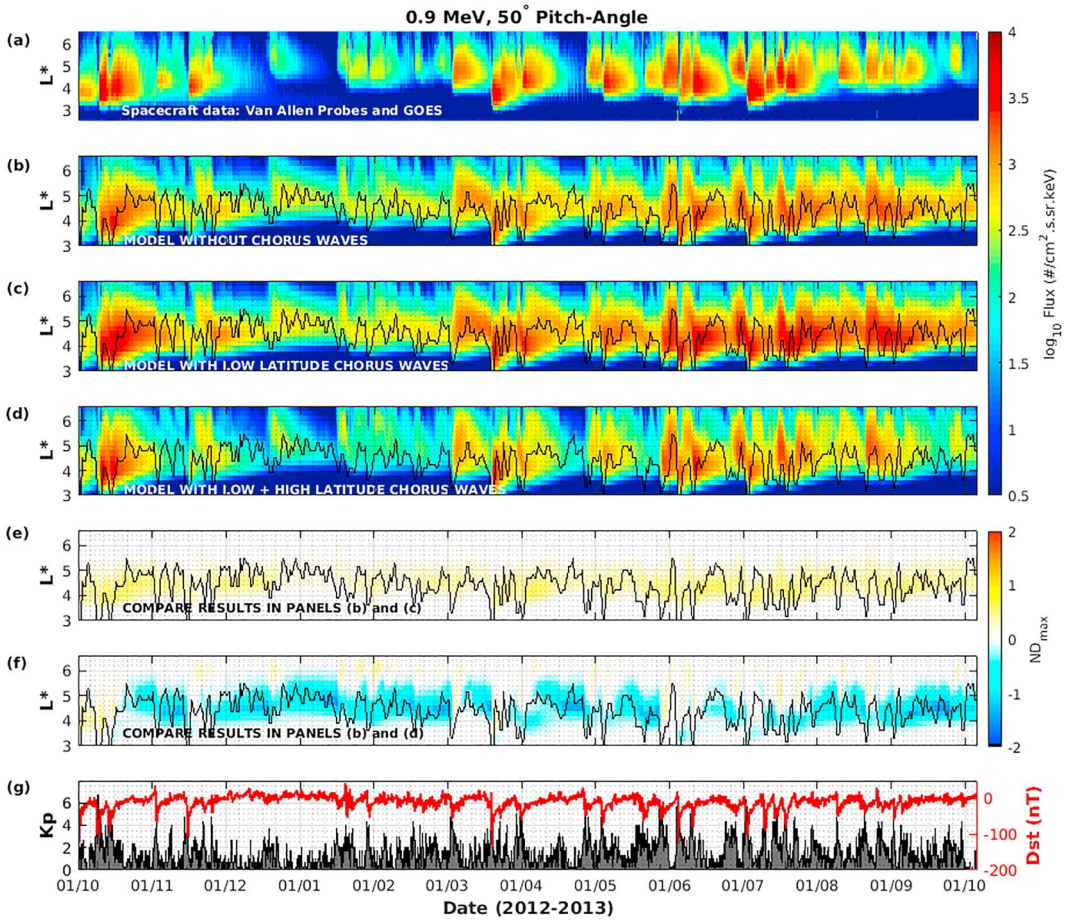

Figure 2. Flux of electrons with an energy of 0.9 MeV and pitch angle of 50° from observations (a), simulation without chorus waves (b), simulation with low-latitude chorus waves (c), and simulation with both low- and high-latitude chorus waves (d). (e) The differences between the results shown in panel (c) and panel (b) normalized by the average maximum flux for each given time. (f) The differences between the results shown in panel (c) and panel (b) normalized by the average maximum flux for each given time. (g) *Dst* (red) and *Kp* (black) index adopted from Figure 1f.

20°. For the second simulation, in addition to low-latitude chorus waves, we include high-latitude chorus waves following the assumptions described in section 2.1. Results of the simulations are validated against the observations from the Van Allen Probes and the GOES satellites, which are presented as follows.

The Magnetic Electron Ion Spectrometer instruments on board the Van Allen Probes measure electrons with energies from 20 keV to several MeV (Blake et al., 2013). Figure 1 shows the particle observation and VERB-3D simulations from 1 October 2012 to 1 October 2013. Figure 1a illustrates the flux of electrons with an energy of 0.9 MeV and pitch angle of 50°, from observations of the Van Allen Probes and GOES 13 and 15. Here, L^* is the Roederer L parameter associated with the third adiabatic invariant (Roederer, 1970) and is calculated using the TS07D magnetic field model (Tsyganenko & Sitnov, 2007). Depending on different geomagnetic conditions, the L^* of particles measured by satellites can be different. During the year that we investigated in this study, the L^* of GOES satellites extended as far outward as 10 and as far inward as 5, and the L^* of Van Allen Probes extended as far outward as 7. To make the comparisons between the satellite data and the simulation results more convenient, we averaged the satellite data into the same grid as in the simulation output. The grid has the time step of 12 hr and L^* step of 0.2. Data from GOES and the Van Allen Probes show a good agreement with each other at conjunction points. Both GOES and the Van Allen Probes observe some significant enhancements and dropouts of relativistic electrons during this 1-year period. Figure 1b shows results of the first simulation using chorus waves limited to low latitudes ($|\lambda| \leq 20°$). In other words, there are no chorus waves at high latitudes in Simulation 1. The plasmapause location (overplotted as a black line) calculated using equation (4) is separating the assumed scattering by

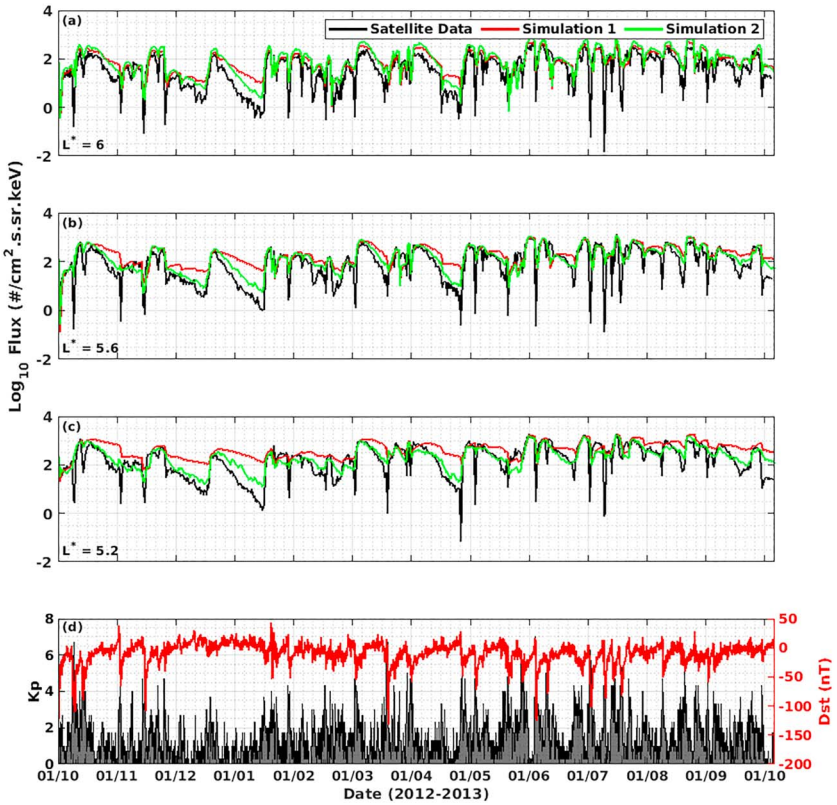

Figure 3. Flux of electrons with an energy of 0.9 MeV and pitch angle of 50° from observations (black lines), Simulation 1 (red lines), and Simulation 2 (green lines) at $L^* = 6$ (a), 5.6 (b), and 5.2 (c). (d) *Dst* (red) and *Kp* (black) index adopted from Figure 1f.

chorus waves and hiss waves. It can be seen that, overall, this simulation reproduced the dynamic evolution of relativistic electrons with energy 0.9 MeV and pitch angle 50°. Figure 1c shows the results of Simulation 2 using the chorus wave model from Van Allen Probe observations (Wang et al., 2019) at low latitudes, and extending chorus waves to high latitudes with scaled amplitudes in different geomagnetic conditions as described above. It can be seen that, using this assumption, the agreement between the simulations and observations has been significantly improved. Figures 1d and 1e show the normalized difference between satellite observations and Simulation 1 and Simulation 2, respectively. Red and yellow colors illustrate where the simulation results overestimate the observations, and the blue color shows where the simulations underestimate the observations. Note that magnetic field models may result in significant errors during storms, which may cause some disagreement around the minimum *Dst* value. Figure 1d shows that Simulation 1 produces an overestimation of the satellite measurements, especially during the quiet time. This result may suggest that an unrealistic limitation of chorus waves to low latitudes did not reproduce enough loss during quiet times. Comparing Figure 1d with Figure 1e, it is clear that the agreement between satellite observations and simulation results is improved in Simulation 2. It is interesting that, although the different factors between these simulations are chorus waves outside the plasmapause, significant differences occur not only outside the plasmapause, but also inside the plasmapause. This can also be seen in the logarithmic differences (Figure S2), especially in the differences normalized by the average maximum flux for each given time (Figure S3). This is due to the effect of radial diffusion. High-latitude chorus waves produce gradients of PSD at higher L shells, and then radial diffusion moves particles outward. Simulations including activity-dependent high-latitude chorus waves can better capture the variability of MeV electrons in different geomagnetic conditions than simulations with constant dependence of chorus waves on latitude. There is still some overestimation of the flux inside the plasmapause, which may be due to the underestimation of hiss-induced loss inside the plasmapause. Figure 1f displays the *Dst* and *Kp* index, showing the geomagnetic condition during this period. It can be seen that the improvement of Simulation 2 in comparison to Simulation 1 mainly occurs during quiet geomagnetic conditions.

We also performed simulations without chorus waves, and the results are shown in Figure 2b. To compare the results with those shown in Figure 1, we repeat Figures 1a–1c as Figures 2a, 2c, and 2d. As one can see from Figure 2b, loss can be produced in the simulation that completely ignores chorus scattering. Thus, decreases in fluxes in simulations should not necessarily be interpreted as chorus producing losses. Such loss can be produced by magnetopause shadowing, outward diffusion, and hiss waves. Figure 2e shows the differences between the results shown in panel (c) and panel (b) normalized by the average maximum flux for each given time. Figure 2f shows the differences between the results shown in panel (d) and panel (b) normalized by the average maximum flux for each given time. It can be seen from Figure 2e that adding low-latitude chorus waves into the simulation results in more acceleration. Then, Figure 2f shows that adding high-latitude chorus waves during quiet times in the simulation tips the balance between acceleration and loss of MeV electrons toward a net loss. On the other hand, during storm times, decreasing of high latitude tips the balance toward acceleration. To show the effect of high-latitude chorus waves more clearly, 3-D simulations under assumed geomagnetic conditions are performed, and results are shown in Figure S4 in the supporting information. It can be seen from these figures that, during a sustained quiet time after a storm, high-latitude chorus waves tip the balance between acceleration and loss of MeV electrons toward a net loss.

To compare the simulation results with the observations in more detail, we plot fluxes at specific L shells in Figure 3. The word "L shells" in this paper means the Roederer L parameter (L^*), which is associated with the third adiabatic invariant (Roederer, 1970), but not the McIlwain L parameter. Figures 3a–3c show the flux of electrons with an energy of 0.9 MeV and pitch angle of 50° from observations (black lines), Simulation 1 (red lines), and Simulation 2 (green lines) at $L^* = 6$, 5.6, and 5.2, respectively. The regions with these L shells are outside the plasmapause most of the time during the year studied here. The sharp drops in the observations are related to the adiabatic changes, which are not accurately described by the used magnetic field model. Inclusion of high-latitude chorus waves improves the agreement between observed and modeled decay rates at quiet geomagnetic conditions and during storm recovery phase. Electron fluxes with an energy of 0.9 MeV and pitch angles of 20° and 80° are shown in the supporting information (Figures S5–S8). Simulation results and comparisons with satellite data for electrons at 500-keV energy and 50° pitch angle are shown in Figure S9. Readers may notice in Figure 3 that sometimes results from simulation including high-latitude chorus waves (green lines) give higher flux than those from simulation without high-latitude chorus waves (red lines). To understand this phenomenon, we performed 2-D simulations with and without high-latitude chorus waves at these high L shells. One example of the results is shown in Figure S10. Results show that this phenomenon is attributed to the combination of the fast redistribution across pitch angles and slow energy diffusion near the 50° pitch angle, as one can see from the diffusion coefficients shown in Figure S1. It takes several days to change the net effect from acceleration to loss. This process takes longer time at higher L shells than it does at lower L shells. These results show that it is difficult to predict the outcome of the competition of acceleration and loss by simple comparison between energy and pitch angle diffusion coefficients. The net effect of chorus waves depends not only on the energy and pitch angle diffusion coefficients but also on the gradient of the PSD and mixed diffusion. To evaluate the net effect, simulations including energy, pitch angle, and mixed diffusion coefficients are needed.

4. Discussion and Conclusions

In this paper, we performed simulations to test the effect of chorus waves at high latitudes. Results show that the distribution of chorus waves at latitudes higher than 20° plays a critical role for the dynamic evolution of radiation belt electrons at MeV energies. Simulation with high-latitude chorus waves reproduces variability of MeV electrons well during multiple storm time and quiet time periods. During disturbed periods, chorus waves mainly contribute to the acceleration of relativistic electrons, while during quiet geomagnetic conditions when waves may extend to high latitudes, the net effect of chorus is likely loss of MeV electrons. However, it is difficult to make definitive predictions, since chorus waves at latitudes higher than 20° have not been well quantified. A statistical study using Cluster data (see Figure 5 in Agapitov et al., 2018) indicates that chorus waves at high latitudes may be strongly damped when $Kp > 4$, but this trend is not very clear due to the limited number of available measurements. Wave measurements from the Exploration of energization and Radiation in Geospace (ERG) mission at high latitudes may be helpful for future quantification of the effects associated with high-latitude chorus. Developing a chorus wave model combining Van Allen Probe and ERG measurements and all other available sources of data will be a subject of future research.

Another potential explanation for the observed decays of the radiation belt electron fluxes outside the plasmasphere during quiet geomagnetic conditions is that there is another missing physical mechanism. However, this potential missing mechanism is difficult to pinpoint until a more accurate analysis of the effects of high-latitude chorus is performed. If the distribution of chorus waves at high latitudes is not as we have assumed in this study, some additional potential mechanisms may play a role in the dynamic of relativistic electrons and need to be carefully quantified. The variation of background electron number density can potentially influence the dynamics of wave-particle interactions during different geomagnetic conditions. Investigation of the effect of electron number density in the background during different geomagnetic conditions will be a subject of future study. Apart from the magnetosphere of the Earth, chorus waves at high latitudes on the other planets also need further investigation. By performing calculations of diffusion coefficients, Shprits et al. (2012) showed that depending on the latitudinal extent of waves, chorus waves may produce net acceleration or loss on both Jupiter and Saturn. Chorus wave measurements at high latitudes in the magnetospheres of Jupiter from satellites such as Juno will help us to improve our understanding of the effects of chorus waves at high latitudes. In particular, the presence of strong waves at high latitudes may indicate that chorus waves are incapable of producing a net acceleration of electrons.

Acknowledgments
All Van Allen Probes data used in this study were accessed through the website https://rbsp-ect.lanl.gov, and we graciously thank the MagEIS instrument team. The *Kp* index was provided by GFZ Section 2.3 and downloaded from the World Data Center (http://wdc.kugi.kyoto-u.ac.jp/). The *Dst* index was downloaded from the SPDF OMNI web. We sincerely acknowledge Adam Kellerman for the preparation of the used satellite data and the calculation of the last closed drift shell. We would like to thank Alexander Drozdov, Nikita Aseev, and Hayley Allison for the useful discussions. We are grateful to Sharon Uy and Dominika Boneberg for the help with editing the paper. We acknowledge the reviewers for their insightful comments and suggestions, which helped to improve this paper. This project has received funding from the European Union's Horizon 2020 research and innovation programme under grant agreement 637302, NASA H-SR funding NNX15AI94G, Iowa NASA subcontract Iowa/NASA 1000933166 NNX11AM36G, and the Helmholtz-Gemeinshaft (HGF) [https://doi.org/10.13039/501100001656].

References

Agapitov, O. V., Artemyev, A. V., Mourenas, D., Mozer, F. S., & Krasnoselskikh, V. (2015). Empirical model of lower band chorus wave distribution in the outer radiation belt. *Journal of Geophysical Research: Space Physics*, *120*, 10,425–10,442. https://doi.org/10.1002/2015JA021829

Agapitov, O. V., Mourenas, D., Artemyev, A. V., Mozer, F. S., Hospodarsky, G., Bonnell, J., & Krasnoselskikh, V. (2018). Synthetic empirical chorus wave model from combined Van Allen Probes and Cluster statistics. *Journal of Geophysical Research: Space Physics*, *123*, 297–314. https://doi.org/10.1002/2017JA024843

Allison, H. J., Horne, R. B., Glauert, S. A., & Del Zanna, G. (2019). On the importance of gradients in the low energy electron phase space density for relativistic electron acceleration. *Journal of Geophysical Research: Space Physics*, *124*, 2628–2642. https://doi.org/10.1029/2019JA026516

Artemyev, A., Agapitov, O., Mourenas, D., Krasnoselskikh, V., Shastun, V., & Mozer, F. (2016). Oblique whistler-mode waves in the Earth's inner magnetosphere: Energy distribution, origins, and role in radiation belt dynamics. *Space Science Reviews*, *200*(1-4), 261–355.

Blake, J. B., Carranza, P. A., Claudepierre, S. G., Clemmons, J. H., Crain, W. R., Dotan, Y., et al. (2013). The magnetic electron ion spectrometer (MagEIS) instruments aboard the radiation belt storm probes (RBSP) spacecraft, *The Van Allen Probes mission* (pp. 383–421). Switzerland: Springer.

Brautigam, D. H., & Albert, J. M. (2000). Radial diffusion analysis of outer radiation belt electrons during the October 9, 1990, magnetic storm. *Journal of Geophysical Research*, *105*(A1), 291–309.

Boscher, D., Bourdarie, S., O'Brien, P., & Guild, T. (2010). IRBEM library v4.3, 2004–2008. Washington, DC: ONERA-DESP, Toulouse France, Aerospace Corporation.

Bunch, N. L., Spasojevic, M., Shprits, Y. Y., Gu, X., & Foust, F. (2013). The spectral extent of chorus in the off-equatorial magnetosphere. *Journal of Geophysical Research: Space Physics*, *118*, 1700–1705. https://doi.org/10.1029/2012JA018182

Cao, X., Shprits, Y. Y, Ni, B., & Zhelavskaya, I. S. (2017). Scattering of ultra-relativistic electrons in the Van Allen radiation belts accounting for hot plasma effects. *Scientific Reports*, *7*(1), 17719.

Carpenter, D. L., & Anderson, R. R. (1992). An ISEE/whistler model of equatorial electron density in the magnetosphere. *Journal of Geophysical Research*, *97*(A2), 1097–1108.

Chen, L., Thorne, R. M., Li, W., & Bortnik, J. (2013). Modeling the wave normal distribution of chorus waves. *Journal of Geophysical Research: Space Physics*, *118*, 1074–1088. https://doi.org/10.1029/2012JA018343

Drozdov, A. Y., Shprits, Y. Y., Aseev, N. A., Kellerman, A. C., & Reeves, G. D. (2017). Dependence of radiation belt simulations to assumed radial diffusion rates tested for two empirical models of radial transport. *Space Weather*, *15*, 150–162. https://doi.org/10.1002/2016SW001426

Drozdov, A. Y., Shprits, Y. Y., Orlova, K. G., Kellerman, A. C., Subbotin, D. A., Baker, D. N., et al. (2015). Energetic, relativistic, and ultra-relativistic electrons: Comparison of long-term verb code simulations with Van Allen Probes measurements. *Journal of Geophysical Research: Space Physics*, *120*, 3574–3587. https://doi.org/10.1002/2014JA020637

Horne, R. B., Kersten, T., Glauert, S. A., Meredith, N. P., Boscher, D., Sicard-Piet, A., et al. (2013). A new diffusion matrix for whistler mode chorus waves. *Journal of Geophysical Research: Space Physics*, *118*, 6302–6318. https://doi.org/10.1002/jgra.50594

Horne, R. B., & Thorne, R. M. (1998). Potential waves for relativistic electron scattering and stochastic acceleration during magnetic storms. *Geophysical Research Letters*, *25*(15), 3011–3014. https://doi.org/10.1029/98GL01002

Horne, R. B., & Thorne, R. M. (2003). Relativistic electron acceleration and precipitation during resonant interactions with whistler-mode chorus. *Geophysical research letters*, *30*(10), 1527. https://doi.org/10.1029/2003GL016973

Horne, R. B., Thorne, R. M., Shprits, Y. Y., Meredith, N. P., Glauert, S. A., Smith, A. J., et al. (2005). Wave acceleration of electrons in the Van Allen radiation belts. *Nature*, *437*(7056), 227–230.

Kersten, T., Horne, R. B., Glauert, S. A., Meredith, N. P., Fraser, B. J., & Grew, R. S. (2014). Electron losses from the radiation belts caused by EMIC waves. *Journal of Geophysical Research: Space Physics*, *119*, 8820–8837. https://doi.org/10.1002/2014JA020366

Kim, K.-C., Shprits, Y., Subbotin, D., & Ni, B. (2012). Relativistic radiation belt electron responses to GEM magnetic storms: Comparison of CRRES observations with 3-D VERB simulations. *Journal of Geophysical Research*, *117*, A08221. https://doi.org/10.1029/2011JA017460

Lenchek, A. M., & Singer, S. F. (1962). Geomagnetically trapped protons from cosmic-ray albedo neutrons. *Journal of Geophysical Research*, *67*(4), 1263–1287.

Li, W., Shprits, Y. Y., & Thorne, R. M. (2007). Dynamic evolution of energetic outer zone electrons due to wave-particle interactions during storms. *Journal of Geophysical Research*, *112*, A10220. https://doi.org/10.1029/2007JA012368

Meredith, N. P., Horne, R. B., Sicard-Piet, A., Boscher, D., Yearby, K. H., Li, W., & Thorne, R. M. (2012). Global model of lower band and upper band chorus from multiple satellite observations. *Journal of Geophysical Research*, *117*, A10225. https://doi.org/10.1029/2012JA017978

Meredith, N. P., Horne, R. B., Thorne, R. M., & Anderson, R. R. (2003). Favored regions for chorus-driven electron acceleration to relativistic energies in the Earth's outer radiation belt. *Geophysical Research Letters*, *30*(16), 1871. https://doi.org/10.1029/2003GL017698

Meredith, N. P., Horne, R. B., Thorne, R. M., Summers, D., & Anderson, R. R. (2004). Substorm dependence of plasmaspheric hiss. *Journal of Geophysical Research*, *109*, A06209. https://doi.org/10.1029/2004JA010387

Millan, R. M., & Baker, D. N. (2012). Acceleration of particles to high energies in Earth's radiation belts. *Space Science Reviews*, *173*(1-4), 103–131. https://doi.org/10.1007/s11214-012-9941-x

Ni, B., Thorne, R. M., Shprits, Y. Y., & Bortnik, J. (2008). Resonant scattering of plasma sheet electrons by whistler-mode chorus: Contribution to diffuse auroral precipitation. *Geophysical Research Letters*, *35*, L11106. https://doi.org/10.1029/2008GL034032

Orlova, K. G., & Shprits, Y. Y. (2011). On the bounce-averaging of scattering rates and the calculation of bounce period. *Physics of Plasmas*, *18*(9), 092904.

Orlova, K., Shprits, Y., & Spasojevic, M. (2016). New global loss model of energetic and relativistic electrons based on Van Allen Probes measurements. *Journal of Geophysical Research: Space Physics*, *121*, 1308–1314. https://doi.org/10.1002/2015JA021878

Ozeke, L. G., Mann, I. R., Murphy, K. R, Jonathan Rae, I., & Milling, D. K. (2014). Analytic expressions for ULF wave radiation belt radial diffusion coefficients. *Journal of Geophysical Research: Space Physics*, *119*, 1587–1605. https://doi.org/10.1002/2013JA019204

Reeves, G. D., Spence, H. E., Henderson, M. G., Morley, S. K., Friedel, R. H. W., Funsten, H. O., et al. (2013). Electron acceleration in the heart of the Van Allen radiation belts. *Science*, *341*(6149), 991–994.

Roederer, J. G. (1970). *Dynamics of geomagnetically trapped radiation* (1st ed., vol. 2). New York: Springer-Verlag Berlin Heidelberg.

Santolík, O., Macúšová, E., Kolmašová, I., Cornilleau-Wehrlin, N., & de Conchy, Y. (2014). Propagation of lower-band whistler-mode waves in the outer Van Allen belt: Systematic analysis of 11 years of multi-component data from the Cluster spacecraft. *Geophysical Research Letters*, *41*, 2729–2737. https://doi.org/\ignorespaces10.1002/2014GL059815

Schulz, M., & Lanzerotti, L. J. (1974). *Particle diffusion in the radiation belts* (Vol. 7). New York: Springer Science & Business Media.

Shprits, Y. Y., Drozdov, A. Y., Spasojevic, M., Kellerman, A. C., Usanova, M. E., Engebretson, M. J., et al. (2016). Wave-induced loss of ultra-relativistic electrons in the Van Allen radiation belts. *Nature communications*, *7*, 12883.

Shprits, Y. Y., Kellerman, A., Aseev, N., Drozdov, A. Y., & Michaelis, I. (2017). Multi-MeV electron loss in the heart of the radiation belts. *Geophysical Research Letters*, *44*, 1204–1209. https://doi.org/10.1002/2016GL072258

Shprits, Y. Y., Menietti, J. D., Gu, X., Kim, K.-C., & Horne, R. B. (2012). Gyroresonant interactions between the radiation belt electrons and whistler mode chorus waves in the radiation environments of Earth, Jupiter, and Saturn: A comparative study. *Journal of Geophysical Research*, *117*, A11216. https://doi.org/10.1029/2012JA018031

Shprits, Y. Y., & Ni, B. (2009). Dependence of the quasi-linear scattering rates on the wave normal distribution of chorus waves. *Journal of Geophysical Research*, *114*, A11205. https://doi.org/10.1029/2009JA014223

Shprits, Y. Y., Subbotin, D., Drozdov, A., Usanova, M. E., Kellerman, A., Orlova, K., et al. (2013). Unusual stable trapping of the ultrarelativistic electrons in the Van Allen radiation belts. *Nature Physics*, *9*(11), 699–703.

Shprits, Y. Y., Subbotin, D. A., Meredith, N. P., & Elkington, S. R. (2008). Review of modeling of losses and sources of relativistic electrons in the outer radiation belt II: Local acceleration and loss. *Journal of Atmospheric and Solar-Terrestrial Physics*, *70*(14), 1694–1713.

Shprits, Y. Y., Subbotin, D., & Ni, B. (2009). Evolution of electron fluxes in the outer radiation belt computed with the VERB code. *Journal of Geophysical Research*, *114*, A11209. https://doi.org/10.1029/2008JA013784

Shprits, Y. Y., Thorne, R. M., Horne, R. B., & Summers, D. (2006). Bounce-averaged diffusion coefficients for field-aligned chorus waves. *Journal of Geophysical Research*, *111*, A10225. https://doi.org/10.1029/2006JA011725

Spasojevic, M., Shprits, Y. Y., & Orlova, K. (2015). Global empirical models of plasmaspheric hiss using Van Allen Probes. *Journal of Geophysical Research: Space Physics*, *120*, 10,370–10,383. https://doi.org/10.1002/2015JA021803

Su, Z., Xiao, F., Zheng, H., He, Z., Zhu, H., Zhang, M., et al. (2014). Nonstorm time dynamics of electron radiation belts observed by the Van Allen Probes. *Geophysical Research Letters*, *41*, 229–235. https://doi.org/10.1002/2013GL058912

Subbotin, D. A., Shprits, Y. Y., & Ni, B. (2011). Long-term radiation belt simulation with the VERB 3-D code: Comparison with CRRES observations. *Journal of Geophysical Research*, *116*, A12210. https://doi.org/10.1029/2011JA017019

Summers, D., Thorne, R. M., & Xiao, F. (1998). Relativistic theory of wave-particle resonant diffusion with application to electron acceleration in the magnetosphere. *Journal of Geophysical Research*, *103*(A9), 20,487–20,500. https://doi.org/10.1029/98JA01740

Thorne, R. M. (2010). Radiation belt dynamics: The importance of wave-particle interactions. *Geophysical Research Letters*, *37*, L22107. https://doi.org/10.1029/2010GL044990

Thorne, R. M., Li, W., Ni, B., Ma, Q., Bortnik, J., Chen, L., et al. (2013). Rapid local acceleration of relativistic radiation-belt electrons by magnetospheric chorus. *Nature*, *504*(7480), 411–414.

Thorne, R. M., O'Brien, T. P., Shprits, Y. Y., Summers, D., & Horne, R. B. (2005). Timescale for MeV electron microburst loss during geomagnetic storms. *Journal of Geophysical Research*, *110*, A09202. https://doi.org/10.1029/2004JA010882

Tsurutani, B. T., & Smith, E. J. (1977). Two types of magnetospheric ELF chorus and their substorm dependences. *Journal of Geophysical Research*, *82*(32), 5112–5128.

Tsyganenko, N. A., & Sitnov, M. I. (2007). Magnetospheric configurations from a high-resolution data-based magnetic field model. *Journal of Geophysical Research*, *112*, A06225. https://doi.org/10.1029/2007JA012260

Tu, W., Cunningham, G. S., Chen, Y., Henderson, M. G., Camporeale, E., & Reeves, G. D. (2013). Modeling radiation belt electron dynamics during GEM challenge intervals with the DREAM3D diffusion model. *Journal of Geophysical Research: Space Physics*, *118*, 6197–6211. https://doi.org/10.1002/jgra.50560

Turner, D. L., Angelopoulos, V., Li, W., Bortnik, J., Ni, B., Ma, Q., et al. (2014). Competing source and loss mechanisms due to wave-particle interactions in Earth's outer radiation belt during the 30 September to 3 October 2012 geomagnetic storm. *Journal of Geophysical Research: Space Physics*, *119*, 1960–1979. https://doi.org/10.1002/2014JA019770

Usanova, M. E., Drozdov, A., Orlova, K., Mann, I. R., Shprits, Y., Robertson, M. T., et al. (2014). Effect of EMIC waves on relativistic and ultrarelativistic electron populations: Ground-based and Van Allen Probes observations. *Geophysical Research Letters*, *41*, 1375–1381. https://doi.org/10.1002/2013GL059024

Wang, D., Shprits, Y. Y., Zhelavskaya, I. S., Agapitov, O. V., Drozdov, A. Y., & Aseev, N. A. (2019). Analytical chorus wave model derived from Van Allen Probe observations. *Journal of Geophysical Research: Space Physics*, *124*, 1063–1084. https://doi.org/10.1029/2018JA026183

Wang, D. D., Yuan, Z. G., Deng, X. H., Zhou, M., Huang, S., Li, M., et al. (2014). Compression-related EMIC waves driverelativistic electron precipitation. *Science China Technological Sciences*, *57*, 2418–2425. https://doi.org/10.1007/s11431-014-5701-3

Xiao, F., Su, Z., Zheng, H., & Wang, S. (2009). Modeling of outer radiation belt electrons by multidimensional diffusion process. *Journal of Geophysical Research*, *114*, A03201. https://doi.org/10.1029/2008JA013580

Xiao, F., Su, Z., Zheng, H., & Wang, S. (2010). Three-dimensional simulations of outer radiation belt electron dynamics including cross-diffusion terms. *Journal of Geophysical Research*, *115*, A05216. https://doi.org/10.1029/2009JA014541

Xiao, F., Yang, C., He, Z., Su, Z., Zhou, Q., He, Y., et al. (2014). Chorus acceleration of radiation belt relativistic electrons during March 2013 geomagnetic storm. *Journal of Geophysical Research: Space Physics*, *119*, 3325–3332. https://doi.org/10.1002/2014JA019822

Xiao, F., Yang, C., Su, Z., Zhou, Q., He, Z., He, Y., et al. (2015). Wave-driven butterfly distribution of Van Allen belt relativistic electrons. *Nature communications*, *6*, 8590.